Lagrangian Data Assimilation in Multilayer Primitive Equation Ocean Models

ANNE MOLCARD

RSMAS/MPO, University of Miami, Miami, Florida, and CNR ISAC-TO, Torino, Italy

ANNALISA GRIFFA

RSMAS/MPO, University of Miami, Miami, Florida, and CNR ISMAR-SP, La Spezia, Italy

TAMAY M. ÖZGÖKMEN

RSMAS/MPO, University of Miami, Miami, Florida

(Manuscript received 4 November 2003, in final form 2 June 2004)

ABSTRACT

Because of the increases in the realism of OGCMs and in the coverage of Lagrangian datasets in most of the world's oceans, assimilation of Lagrangian data in OGCMs emerges as a natural avenue to improve ocean state forecast with many potential practical applications, such as environmental pollutant transport, biological, and naval-related problems.

In this study, a Lagrangian data assimilation method, which was introduced in prior studies in the context of single-layer quasigeostrophic and primitive equation models, is extended for use in multilayer OGCMs using statistical correlation coefficients between velocity fields in order to project the information from the data-containing layer to the other model layers. The efficiency of the assimilation scheme is tested using a set of twin experiments with a three-layer model, as a function of the layer in which the floats are launched and of the assimilation sampling period normalized by the Lagrangian time scale of motion.

It is found that the assimilation scheme is effective provided that the correlation coefficient between the layer that contains the data and the others is high, and the data sampling period Δt is smaller than the Lagrangian time scale T_L. When the assimilated data are taken in the first layer, which is the most energetic and is characterized by the fastest time scale, the assimilation is very efficient and gives relatively low errors also in the other layers ($\approx$ 40% in the first 120 days) provided that Δt is small enough, $\Delta t << T_L$. The assimilation is also efficient for data released in the third layer (errors $<$ 60%), while the dependence on Δt is distinctively less marked for the same range of values, since the time scales of the deeper layer are significantly longer. Results for the intermediate layer show a similar insensitivity to Δt, but the errors are higher (exceeding 70%), because of the lower correlation with the other layers. These results suggest that the assimilation of deep-layer data with low energetics can be very effective, but it is strongly dependent on layer correlation. The methodology also remains quite robust to large deviations from geostrophy.

1. Introduction

Near–real-time satellite and in situ observations play a fundamental role in operational programs [e.g., the Global Ocean Observing System (GOOS), Climate Variability and Predictability (CLIVAR), the Mediterranean Forecasting System Toward Environmental Predictions (MFSTEP), Atlantic Circulation and Climate Experiment (ACCE), ARGO], and have allowed drastic improvement of ocean forecast capabilities. Satellite data, such as sea surface height (SSH), are routinely assimilated in operational ocean general circulation models (OGCMs) (e.g., Oschlies and Willebrand 1996; Cooper and Haines 1996; Killworth et al. 2001; Masina et al. 2001; Robinson and Lermusiaux 2001; Demirov et al. 2003), while in situ data such as temperature (T) and salinity (S) profiles are often used to provide information on the state of the interior ocean (Greiner and Arnault 2000; Thacker and Esenkov 2002; Li et al. 2003; Raicich and Rampazzo 2003).

In the last few years, there has been a growing interest (Mariano et al. 2002) in the development of new assimilation schemes including Lagrangian data, that is, floating buoy positions to correct the Eulerian velocity fields forecasted by models. Lagrangian datasets have reached a critical mass in most of the world's oceans (e.g., Davis 1991; Owens 1991; Lavender et al. 2000; Fratantoni 2001; Richardson 2001; Zhang et al. 2001; Bauer et al. 2002; Zhou et al. 2002; Reverdin et al. 2003)

Corresponding author address: Dr. Tamay M. Özgökmen, MPO Division, The Rosenstiel School, University of Miami, 4600 Rickenbacker Causeway, Miami, FL 33149-1098.
E-mail: tozgokmen@rsmas.miami.edu

in terms of both surface drifters and deep ocean profiling floats (Davis et al. 1992, 2001; Lavender et al. 2002). These floats are programmed to drift freely at a nominal depth z_n for a fixed time period typically of the order of 3–15 days, after which they ascend to the surface and communicate via satellite information on position and *T*/*S* profiles. While the primary use of these profiling floats is presently in terms of *T*/*S* assimilation, there is also a clear interest toward position assimilation, even though some questions are still open on how to perform it in an optimal way. Some of the issues, which can be regarded as interesting challenges to address, are specific to the profiler themselves. The meaningful information to correct velocity at the nominal depth z_n is the horizontal displacement experienced by the float at z_n. For profiling floats, which communicate their position only when surfacing, this information is necessarily contaminated by the additional displacement due to vertical shear and surface drift (Davis et al. 1992). Other challenges are more general and common to all Lagrangian data. The main issue is that there is a nonlinear relationship between the observed variable, that is, the position **r**, and the prognostic model variable to be modified, that is, the Eulerian velocity field **u**. This nonlinear relationship enters in the assimilation scheme, introducing significant difficulties in the formulation.

Some earlier studies on Lagrangian data assimilation (e.g., Hernandez et al. 1995; Ishikawa et al. 1996) have circumvented this problem by assuming that the Lagrangian velocity, computed by the finite difference of successive positions $\Delta\mathbf{r}/\Delta t$, can be approximated as an Eulerian velocity and therefore directly assimilated in the OGCM. This approach, denoted "pseudo-Lagrangian," is accurate when the data sampling period Δt is negligible with respect to the Lagrangian time scale T_L, which is typically $\approx$ 1–3 days for ocean surface and $\approx$ 7–15 days for ocean interior (Griffa 1996; Veneziani et al. 2004). On the other hand, when Δt is a sizable fraction of T_L, as is typically the case for ocean measurements, Eulerian and Lagrangian velocities do not coincide and this method becomes inaccurate (Molcard et al. 2003). The Lagrangian nature of the observations has been considered by Carter (1989), who used a Kalman filtering technique, and by Kamachi and O'Brien (1995), who used an adjoint method. In both cases, the path information of Lagrangian data have been considered, but the method implementation is very specific to the considered (simplified) ocean models so that generalization to more complex OGCMs does not appear straightforward.

More recently, a simple, computationally efficient, and highly portable method was developed by Molcard et al. (2003) based on optimal interpolation approach, which rigorously takes into account the Lagrangian nature of the observations, namely, the fact that they are particle positions or, equivalently, time integrals of particle velocities. The Eulerian velocity field correction is obtained by minimizing the distance between observed positions and positions of synthetic floats simulated by the model. The simplest implementation of the method considers only two successive observation points or, equivalently, the Lagrangian velocity over one sample period, $\Delta\mathbf{r}/\Delta t$. This simplified algorithm has been tested and applied to 1.5-layer models in the framework of quasigeostrophic (Molcard et al. 2003) and primitive equation models (Özgökmen et al. 2003). The results show that the method is clearly superior to the pseudo-Lagrangian technique in the parameter range relevant for oceanic observations. Other ongoing efforts include methods based on augmenting the model with a tracer advection equation and tracking the correlations between the flow and the tracers via the extended Kalman filter. This method has given encouraging results for point vortex flows (Ide et al. 2002; Kuznetsov et al. 2003).

Despite the positive results of the method by Molcard et al. (2003) and Özgökmen et al. (2003), applications are still limited with respect to implementation in realistic OGCMs. One of the main limitations is that the method has been so far implemented in models with one active layer, so that the total velocity is directly corrected by the assimilation. In the presence of stratification and multiple layers, the velocity correction has to be propagated vertically in the water column, and the other related dynamical variables, such as pressure or layer thicknesses, have to be consistently modified in all layers.

In this paper, we extend the Lagrangian position assimilation scheme developed in Molcard et al. (2003) and Özgökmen et al. (2003) to models including stratification via multiple layers. In particular, we focus on how to use the information provided by Lagrangian instruments in a given layer (which can be either at the surface or in the ocean interior) by projecting them onto the other layers and the other variables. This is done by using statistical regression coefficients between layer velocities and by correcting layer thickness in each layer using a dynamical balancing technique based on geostrophy and mass conservation. The goal is to provide a general method that is efficient and portable, and that can be applied to surface drifter data as well as to deep float data.

A general approach is proposed and then applied to a three-layer primitive equation Miami Isopycnic Coordinate Ocean Model (MICOM). A simple double-gyre configuration is considered, and experiments are performed in the framework of the classical twin-experiment approach, as in Molcard et al. (2003) and Özgökmen et al. (2003). In the twin experiment approach, a control run is performed, which is regarded as the "true" ocean. Data from the control are assimilated in another run with different characteristics (typically with different initial conditions). If the assimilation is effective, the assimilated run tends to converge toward the control. The approach is obviously highly simplified

with respect to real applications, but it has the advantage that the "truth" is known, so that the assimilation performance can be quantitatively evaluated. The dependence of the assimilation from various parameters, such as the sampling period Δt and the specific layer where the floats are launched, is investigated in detail.

The paper is organized as follows. The methodology is outlined in section 2. In section 3, the experimental setup and the details of the implementation of the assimilation scheme in MICOM are discussed. The results are presented in section 4, and a summary is given in section 5.

2. The methodology

The general method used in this paper can be considered as composed of three successive steps: assimilation of Lagrangian position in a data-containing layer, vertical projection of this information to other layers, and establishment of dynamical compatibility between the corrections to velocity components and those to other prognostic model variables. These steps are summarized and discussed below.

a. Assimilation algorithm for Lagrangian position

The first step consists of using the Lagrangian data to correct the Eulerian model velocity in the same layer where the data are collected. This is done using the same method previously implemented by Molcard et al. (2003) and by Özgökmen et al. (2003) in reduced-gravity models. We summarize below the main aspects of this method for completeness, and the reader is referred to Molcard et al. (2003) for further details.

The general approach is based on considering numerical and observed data with the same importance, and on finding a best combination of them as the optimized ocean forecast. The basic concept of sequential data assimilation (e.g., Ghil and Malanotte-Rizzoli 1991) can be described by

$$\mathbf{u}^a = \mathbf{u}^b + \mathbf{K}[\mathbf{y}^o - \mathbf{H}(\mathbf{u}^b)], \tag{1}$$

where $\mathbf{u}^a$ is the Eulerian model velocity vector after assimilation; $\mathbf{u}^b$ is the model velocity vector before assimilation; $\mathbf{y}$ is the vector of observations; $\mathbf{H}(\mathbf{u}^b)$ is the model counterpart, for example, the measurement functional/model; and $\mathbf{K}$ projects and minimizes the difference between measured and simulated quantities onto the model state space.

Consider M Lagrangian particles released at the same time $t = 0$ from different positions $\mathbf{r}_1^0, \mathbf{r}_2^0, \ldots, \mathbf{r}_M^0$ in an isopycnic layer l. The M particles provide information on their position $\mathbf{r}_m^t$ ($m = 1, M$) at discrete times t with sampling interval Δt. The average Lagrangian velocity during Δt can then be computed by the finite difference of two successive positions, $\mathbf{v}_m(t) = (\mathbf{r}_m^{t+1} - \mathbf{r}_m^t)/\Delta t$ ($m = 1, M$).

In Molcard et al. (2003) and Özgökmen et al. (2003), the Lagrangian velocity information has been used to correct the model Eulerian velocity using the zeroth-order assimilation formula

$$\mathbf{u}_1^a = \mathbf{u}_1^b + \Delta\mathbf{u}_1,$$

with

$$\Delta\mathbf{u}_1(i, j, n) = \alpha^{-1} \sum_{m=1}^{M} \gamma_{ijm}[\mathbf{v}_m^o(n) - \mathbf{v}_m^b(n)]. \tag{2}$$

Here

$$\gamma_{ijm} = E_h[x_m^b(n) - ih, y_m^b(n) - jh],$$

$$E_h(x, y) \equiv \exp\left(-\frac{x^2}{2h^2} - \frac{y^2}{2h^2}\right) \text{ and } \alpha = 1 + \sigma_o^2/\sigma_b^2,$$

where the the indices i, j indicate the Eulerian grid point; n is the discrete time $n\Delta t$; $n = 1, N$; l is the layer in which the Lagrangian particles are released; $\mathbf{v}^o$ and $\mathbf{v}^b$ are the observations (o) and model (b) Lagrangian velocity, respectively; $\mathbf{v}^b$ is computed in the model by generating trajectories during Δt and using the two end points; σ_b^2 is the model velocity mean square error; and σ_o^2 is the error for the Lagrangian velocity that is related to the error of independent positions, say, σ_r^2, by $\sigma_o^2 = \sigma_r^2/\Delta t^2$. It is clear from the expression of α that if the model but not the data velocity error variance goes to zero, there is no correction to be gained [Eq. (2)]. Note that the expression (2) takes into account only one assimilation time step Δt or, equivalently, only two successive data points. In our case, we correct the velocity at time t using drifter positions at time t and $t + 1$. Conceptually, then, it does not fully introduce the information on particle paths. Rather, it converts the position information into Lagrangian velocity information $\mathbf{v}$, that is, velocity averaged along particle trajectories during the time Δt. Even in this zeroth-order approximation, though, the Lagrangian approach is conceptually different from the pseudo-Lagrangian one. In the pseudo-Lagrangian assimilation the functional $\mathbf{H}$ in (1) is linear, so that the the correction term in (1) is computed as the difference between the observed Lagrangian velocity $\mathbf{v}^o$ and the Eulerian model velocity $\mathbf{u}^b$. In the Lagrangian approach (2), instead, the correction is consistently performed, considering the observed and simulated Lagrangian velocities. From the practical point of view, this implies that in the Lagrangian approach, synthetic trajectories are computed in the model to evaluate $\mathbf{v}^b$, which is then compared to $\mathbf{v}^o$. As shown in Molcard et al. (2003) and Özgökmen et al. (2003), the Lagrangian assimilation performs significantly better than the pseudo-Lagrangian one for realistic parameters, and in particular for sizable values of Δt compared to T_L.

In Molcard et al. (2003) and Özgökmen et al. (2003), only one active layer was considered, so that the complete Eulerian velocity was corrected by (2). Here, instead, we consider a multilayer system, where floats are

released in a single layer. The assimilation formula (2), then, is used as a first step in the assimilation, aimed at correcting the Eulerian model velocity in the same layer where the observations are taken. Other steps will be necessary to correct the other layers and variables.

b. Vertical projection of velocity correction

In a multilayer system, the corrections obtained in a single layer need to be projected to the other layers. Since there is no exact analytical relationship between layer velocities, we chose to correct the velocity in layers that do not contain Lagrangian floats using a simple statistical linear regression, with parameters determined empirically. A similar approach has been successfully used by Oschlies and Willebrand (1996), projecting observed corrections of surface geostrophic velocities onto deep velocity corrections.

For each individual column of model grid points, and each velocity component (u, v), we define the vertical regression coefficients as

$$R_{li} = \frac{\langle \delta u_l \delta u_i \rangle}{\langle (\delta u_l)^2 \rangle}, \tag{3}$$

where l is the layer where float positions are measured, and $i = 1, N$ is the layer index. The angle brackets ($\langle\ \rangle$) indicate an ensemble average approximated as a time average, and δu denotes the deviation of the velocity from its mean, which is provided by the model.

The regression coefficient R_{li} is a statistical model to relate two variables, by assuming that a linear relation does exist between them. Assuming that the model corrections on average have the same vertical structure as the model fluctuation velocity, one can estimate the velocity correction in all layers using (3).

In the layer that contains observations, velocities are corrected via (2), while in the layers that contain no data, the velocity is projected using

$$\Delta \mathbf{u}_i = R_{li} \Delta \mathbf{u}_l. \tag{4}$$

In practice, R_{li} are computed considering time averages of model outputs, typically over a 1-yr period or more (e.g., Chin et al. 2002). Also, the R_{li} can be further averaged in space assuming homogeneity, with the advantage of filtering out gravity waves and noise effects. The results of Chin et al. (2002) suggest that spatial averages as wide as the whole basin can provide very satisfactory results, while simplifying the computational problem.

c. Correction of the other prognostic variables

As shown in Özgökmen et al. (2003), the velocity information alone is not adequate in Lagrangian data assimilation, and dynamical compatibility between multiple model variables is an important issue. The strategy used in Özgökmen et al. (2003) for a reduced-gravity model was based on the assumption of geostrophic balance to correct pressure (or layer thickness). A similar approach is used here for the multilayer case.

Let us consider the dynamical relation between model variables,

$$\mathbf{u} = \mathbf{G}(p),$$

where p is the pressure or mass or layer thickness field, depending on the model formulation. Since the operator $\mathbf{G}$ in OGCMs is nonlinear and includes many terms (dissipation, forcing, time dependency, etc.), some assumptions have to be made in order to reduce the complexity of the problem. Conceptually, this is done here assuming the same dynamical balance based on geostrophy and mass conservation that has been used by Özgökmen et al. (2003), which has been found to be very effective for midlatitude ocean circulation. Once a linear relationship is assumed between $\mathbf{u}$ and p, then the same relationship holds also for the respective corrections,

$$\Delta \mathbf{u} = \mathbf{G}(\Delta p). \tag{5}$$

In the following, then, the correction Δp is computed given $\Delta \mathbf{u}$, inverting the linearized operator $\mathbf{G}$. The details of $\mathbf{G}$ depend on the model formulation, so that a detailed description of the method implementation is given in section 3b, after introducing the OGCM.

3. Experimental setup

a. The numerical ocean model

The assimilation method is implemented in MICOM (Bleck and Boudra 1986), which is a primitive equation model with isopycnic vertical coordinate that can be viewed as a stack of shallow-water models, each consisting of momentum and continuity equations:

$$\frac{\partial \mathbf{u}}{\partial t} + \nabla_\rho \frac{\mathbf{u}^2}{2} + (\zeta + f)\boldsymbol{k} \times \mathbf{u} = -\nabla_\rho M - \theta \frac{\partial \boldsymbol{\tau}}{\partial z} + \nu \Delta p^{-1} \nabla_\rho \cdot \Delta p \nabla_\rho \mathbf{u} - \epsilon \mathbf{u}, \tag{6}$$

$$\frac{\partial \Delta p}{\partial t} + \nabla_\rho \cdot (\mathbf{u} \Delta p) = 0,$$

where ζ is the relative vorticity, f is the Coriolis parameter, $M = gz + p\theta$ is the Montgomery potential, $\theta = \rho^{-1}$ is the specific volume, $\boldsymbol{\tau}$ is the wind stress vector, Δp is the pressure difference of the isopycnic layer directly proportional to the layer thickness when considering hydrostaticity, ν is the lateral viscosity, and ϵ is the bottom drag coefficient acting on the lowest layer. The subscript ρ indicates derivatives on surfaces of constant density. The layers communicate vertically through pressure forces. Pressure p and geopotential gz are defined at the interfaces between layers.

The model is set up in an idealized configuration, box domain with a flat bottom and straight sidewalls. No-

flow and free-slip conditions are applied along all lateral boundaries. Three isopycnal layers simulate the vertical density stratification, and the only forcing is a steady zonal wind stress that drives a classic double-gyre circulation. Table 1 summarizes the parameters of the model.

b. Assimilation implementation

The twin experiment approach is used to test the assimilation scheme. In the first experiment (Control) the model is integrated for 10 yr, in order to reach a statistical steady state. Then a set of 24 floats is released in each layer in the energetic region where the meandering jet and the recirculations are present, and advected during a 4-month period. The float positions are considered as ocean data to be assimilated. Even though the floats are launched in all three layers simultaneously, they are used separately in the assimilation experiments; that is, only assimilation of single-layer data is investigated. The choice of float release locations and float density is justified by previous studies (Molcard et al. 2003; Özgökmen et al. 2003; Poje et al. 2002; Toner et al. 2001a,b), which have shown that releasing floats in energetic regions is more efficient than a regular deployment strategy over the whole basin. In Fig. 1, a snapshot of the layer thickness displacement is depicted after 10 yr of integration, as well as the initial drifter positions chosen for the deployment.

The position data are assimilated in the Assim run, which is started from different initial conditions than the Control but has identical parameters otherwise. Finally, the Noassim simulation has the same initial conditions as Assim but no data assimilation, showing the evolution of the model alone and representing our crudest forecast. If the assimilation is successful, the evolution of the corrected forecast (Assim) should be different from Noassim and should converge toward the Control run.

The assimilation is performed implementing the following steps.

1) Synthetic floats are launched in Assim starting from the "real" (from Control) float positions observed at time t, and they are advected for a time interval equal to the sampling period Δt.
2) The velocity correction in the layer where data are measured is computed by minimizing the final distance between real (from Control) and simulated (from Assim) float positions using (2).
3) The velocity correction in the remaining layers is computed using regression coefficients between layers with (3) and (4). The coefficients (3) are averaged over the whole basin, based on preliminary results on assimilation efficiency and in agreement with Chin et al. (2002).
4) The layer thickness is corrected in each layer by inverting (5) and assuming geostrophy. This is implemented in the following way. Combining the two-component momentum equations (6) applied to the model variables corrections, and omitting the ageostrophic terms, we obtain the simple relation (for each layer)

$$\nabla^2(\Delta M_g) = f\left[\frac{\partial(\Delta v)}{\partial x} - \frac{\partial(\Delta u)}{\partial y}\right]. \tag{7}$$

Considering the hydrostatic and Boussinesq approximations, the Montgomery definition can be rewritten in a recursive equation for a layer ocean model (Chin et al. 2002):

$$M_l = M_{l+1} + p_{l+1}(\theta_{l+1} - \theta_l),$$

$$p_{l+1} = p_l + \Delta p_l,$$

where l is the layer index. After inverting (7) using a fast Fourier transform method, the layer thickness corrections in each layer are computed from the Mont-

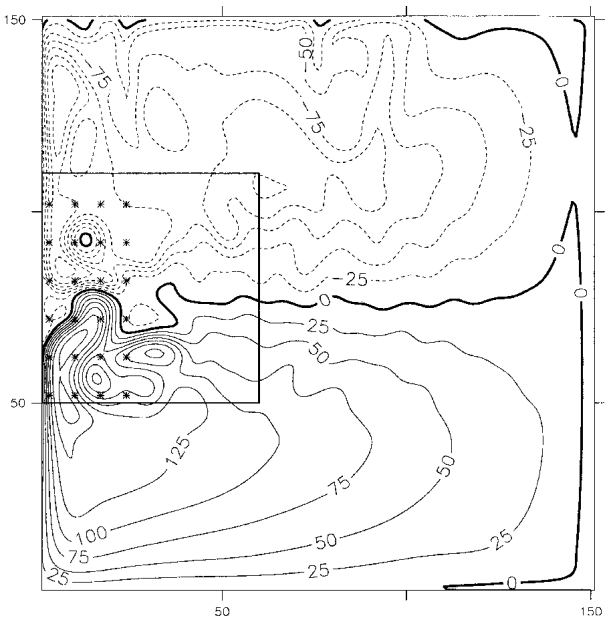

FIG. 1. Snapshot of the Eulerian field of the first-layer thickness displacement ($h - h_{\text{rest}}$) (contour interval: 25 m, with the double-gyre circulation typical structures. The initial condition of 24 drifters launched for the experiments is superimposed on the h field. The box highlights the most energetic region, which is the target region of interest used in the successive figures.

TABLE 1. Parameters of the numerical ocean model simulation.

Basin size (x, y)	3000 km × 3000 km
Horizontal grid scale	$\Delta x = \Delta y = 20$ km
Coriolis parameters	$f_0 = 9.3 \times 10^{-5}\ \text{s}^{-1}$
	$\beta = 2 \times 10^{-11}\ \text{m}^{-1}\ \text{s}^{-1}$
Layer thicknesses	$h_1 = 400$ m $\quad h_2 = 700$ m $\quad h_3 = 4000$ m
Reduced gravities	$g'_{12} = 0.016\ \text{m s}^{-2}$ $\quad g'_{23} = 0.014\ \text{m s}^{-2}$
Lateral viscosity	$\nu = 300\ \text{m}^2\ \text{s}^{-1}$
Bottom friction	$\epsilon = 3 \times 10^{-7}\ \text{s}^{-1}$
Time step	$\delta t = 1200$ s

gomery potential corrections. The correction of pressure (or layer thickness) can have the effect of changing layer mass depending on the sampling positions of synthetic drifters. The mass conservation is satisfied by subtracting the net mass deviation induced by the correction as described in Özgökmen et al. (2003).

c. Error metrics

Finding a valid metric to assess the convergence of assimilation runs toward the Control is an important issue (Miyakoda et al. 1969; Raicich and Rampazzo 2003). The efficiency can be measured in several ways, and the choice has to be made depending on the experimental variability (in space and time) and in order to extract the most information. In this paper we adopt the following metric:

$$\epsilon_{\text{rel}}(l, t) = \frac{\text{ER}_{\text{Control}-\text{Assim}}(l, t)}{\text{ER}_{\text{Control}-\text{Noassim}}(l, t)}, \tag{8}$$

where l indicates the layer and $\text{ER}_{\text{Control-Assim}}$ ($\text{ER}_{\text{Control-Noassim}}$) represents the rms of the velocity difference between Control and Assim (Noassim) defined as

$$\text{ER}_{\text{Control}-\text{Assim}}(l, t) = \sum_A \{[u_{\text{Control}}(l, t) - u_{\text{Assim}}(l, t)]^2 + [v_{\text{Control}}(l, t) - v_{\text{Assim}}(l, t)]^2\}^{1/2},$$

where A is the region of interest, which corresponds to the energetic western region indicated in Fig. 1, surrounding the area where the floats have been launched. The relative error ϵ_{rel} is useful when simulations with different initial conditions are compared, as the evolution of the Noassim run can have a high variability in time. At the initial time, $\epsilon_{\text{rel}} = 1$, and when there is no difference between Control and Assim, $\epsilon_{\text{rel}} = 0$.

The time evolution of $\epsilon_{\text{rel}}(l, t)$ is presented for each layer during the 120 days of simulation, which corresponds to the time scale during which the great majority of the drifters remains within the bounds of the target region and the space sampling density is approximately constant. If $\epsilon_{\text{rel}} < 1$ then the assimilation is successful, and when the slope of the error curve $\partial\epsilon_{\text{rel}}(t)/\partial t$ is negative in average, the assimilation is effective.

d. Characteristics of the experiments

A total of 27 experiments has been performed, the parameters of which are summarized in Table 2. All experiments are performed over a time period of 120 days and they assimilate the trajectories of 24 floats with initial conditions shown in Fig. 1.

TABLE 2. List and characteristics of the 31 runs.

Run	Initial condition	Δt	Launch layer
Control	10Y		
Noassim	11Y, 11.5Y, 12Y		
Assim	11Y, 11.5Y, 12Y	1200 s, 3 days, 6 days	L1, L2, L3

A set of nine benchmark experiments, discussed in detail in section 4, has been first performed using the same initial conditions (for Assim and Noassim), corresponding to the flow configuration after 11 yr of integration (11Y). The nine experiments differ in terms of launching layer for the assimilated float positions and in terms of sampling period Δt. As mentioned in section 3b, the floats are actually simultaneously launched in all three layers, but only single-layer data are considered in each experiment. LaunchL1, LaunchL2, and LaunchL3 denote experiments where floats only from layer 1 (L1), 2 (L2), and 3 (L3), respectively, are used. Three values of Δt are considered: 1200 s (corresponding to the time step of the model), 3 days, and 6 days. Assimilating the float data at each model time step is of course expected to provide the best results, but such a fast sampling is not realistic. Sampling periods of $\Delta t = 3$ and 6 days are more realistic for surface and subsurface floats, respectively, even though these values have to be rescaled in terms of Lagrangian time scale T_L in order to have a meaningful comparison with the data (Molcard et al. 2003). We will come back on this point in the following.

In order to increase the reliability of the results, the number of realizations is increased by repeating the same set of nine experiments starting from two other initial conditions (11.5Y, 12Y), which are characterized by a 6-month lag, that is, corresponding to the 11.5 and 12 yr of integration, respectively. The error metric (8) is presented as an average over the three initial conditions.

4. Results

a. The "true" ocean characteristics

The idealized model configuration gives a classic double-gyre circulation that is highly nonlinear and nonstationary. Figure 2 depicts snapshots of layer thickness and velocity field in the three layers at the initial and final times of the simulation for the Control run in the energetic region (subdomain in Fig. 1). Only the energetic western-central region is considered, as the float positions are measured essentially in this area. The region is characterized by the meandering jet and by ring formation and propagation.

During the 120 days of simulation, the rings move, split, and combine in a rapid way, and the meandering jet is very unsteady. In L1, the boundary current is very intense, while it loses strength with depth (note the velocity magnitude scale in each layer, indicating a factor of 5 between L1 and L2, and a factor of 10 between L1 and L3). Even if the signal is much stronger in L1, most of the main features are present in all layers: the western boundary current and the meandering jet in L1 and L2, and the gyres' centers in L1 and L3. While the

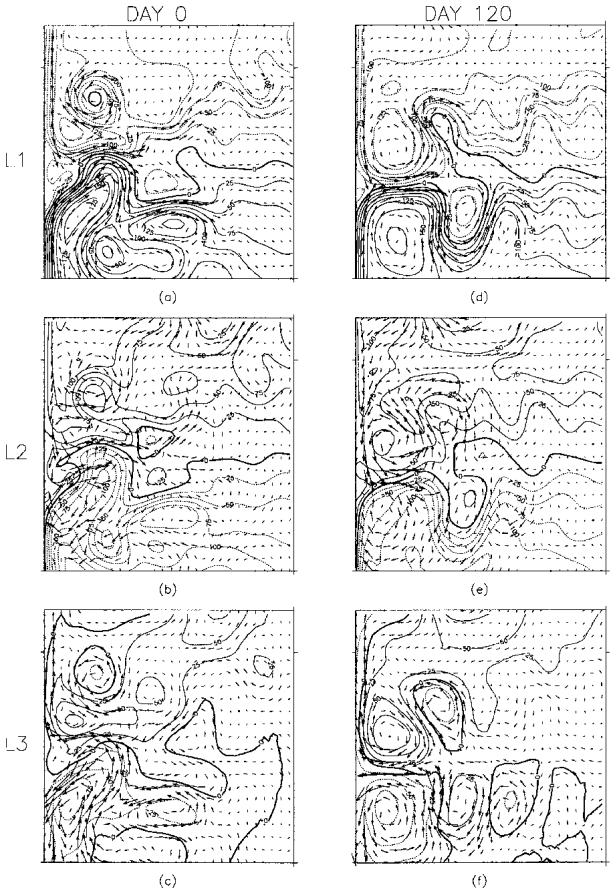

FIG. 2. Control run: layer thickness displacement ($h - h_{\text{rest}}$) superimposed on the velocity field in each layer (L1, L2, L3), at initial time [DAY 0: (a)–(c)] and at the end [DAY 120: (d)–(f)] of the simulation. Contour intervals are 25 m, and the maximum velocity field is approximately 50 cm s^{-1} in L1, 10 cm s^{-1} in L2, and 5 cm s^{-1} in L3.

current is clearly geostrophic in the first layer, the direct balance between the pressure gradient and velocity in the bottom layers is more ambiguous. This is mainly due to the rigid-lid approximation in MICOM, in which the barotropic mass flux divergence is removed from all layer velocities (Bleck and Boudra 1986; Bleck et al. 1989). This term gives an important contribution in the third and second layers and can lead to significant deviations from geostrophy. Notice also that L1 and L3 appear significantly anticorrelated, having the main gyres with opposite layer thickness anomaly sign and corresponding opposite velocity field (Figs. 2a,c and 2d,f), while L2 appears less significantly correlated.

While estimating the vertical regression coefficients (3) from this simulation, the mean flow is computed over a 1-yr period and removed from the velocity field to obtain the deviation δu for each velocity component. The R_{li} values are first computed at all grid points and then spatially averaged over the domain (Chin et al. 2002). Table 3 lists $\overline{R}_{li}$ values used in the vertical projection of velocity corrections. The regression coefficients take into account also the relative magnitude of the velocity field in the layers, unlike the correlation coefficients that indicate only the relative behavior of two fields. Note that $|\overline{R}_{li}|$ can take values greater than unity, indicating that the reference layer where data are measured [l in (3) and (4)] is less energetic. So, for example, the mean velocity field anomaly in layer L1 is more energetic than in L2, with a factor varying from $\overline{R}_{21} = (1.39, 1.40)$ to $\overline{R}_{12}^{-1} = 1/(0.34, 0.24) = (2.9, 4.1)$ (since both regression coefficients link the layers L1 and L2). Since values are positive, L1 and L2 are positively correlated in velocity term, while the negative values indicate that L1 and L3 are anticorrelated, as well as L2 and L3.

TABLE 3. Spatially averaged vertical regression coefficients for each (u, v) velocity component. Each row l corresponds to the launching layer.

$\overline{R}_{li}$	$i = 1$	$i = 2$	$i = 3$
$l = 1$	1	(0.34, 0.24)	(−0.15, −0.13)
$l = 2$	(1.39, 1.40)	1	(−0.28, −0.28)
$l = 3$	(−5.22, −5.43)	(−2.79, −2.67)	1

The regression coefficients are averaged over the whole domain and represent the correlation of the anomaly fields. Preliminary experiments have been done considering different scales of homogeneity in space, by averaging the gridpoint regression coefficients over subregions, and no major differences were found. This is certainly due to the smoothness and large-scale structures of the present field, while for higher-resolution models, some further investigation on the horizontal correlation, and proper spatial averages, should be done.

The correlation coefficients are computed as well, from

$$C_{li} = \frac{\langle \delta u_l \delta u_i \rangle}{\sqrt{\langle \delta u_l^2 \rangle}\sqrt{\langle \delta u_i^2 \rangle}},$$

to get an additional insight in the connection between layers. From (3) it appears that the connection between the regression and the correlation coefficients is the ratio between the covariances. The correlation between layers L1 and L2 is quite weak, reaching a maximum value of 0.5, while the correlation between L1 and L3 is −0.75. This indicates that the eddy field is highly anticorrelated between L1 and L3, suggesting a strong baroclinic component, as for the mean flow. Notice that this result is model dependent and is somewhat unrealistic with respect to the actual eddy field in the Gulf Stream, which tends to be significantly more barotropic than the mean flow.

The efficiency of the vertical projection of the velocity using (4) is very much dependent on the correlation between vertical layers, since the velocity corrections are estimated from it. One can anticipate good results

from assimilating experiments when drifting buoys are launched in either L1 or L3 because the correlation factor between these two layers is high, whereas launching floats in L2 could lead to a less efficient improvement in the forecast.

b. Characteristics of Lagrangian data

The float trajectories are computed integrating the velocity field in the Control run using a second-order Runga–Kutta advection scheme. In Fig. 3 the half-day successive positions of the float measured in each layer from the Control run are plotted in the left-hand panels. As expected, the floats are more energetic in the upper layer, and they travel faster and farther than those in the bottom layers. Even if the data density is higher in the western part, surface floats are traveling in the whole subdomain and are providing more spatial information during the simulation period. As for the velocity fields depicted in Fig. 2, the floats are moving slower in deeper layers, obtaining therefore less spatial information to be assimilated and to improve the forecast. Furthermore, the floats in the three layers are leaving the region of interest, slowly reducing the volume of available information.

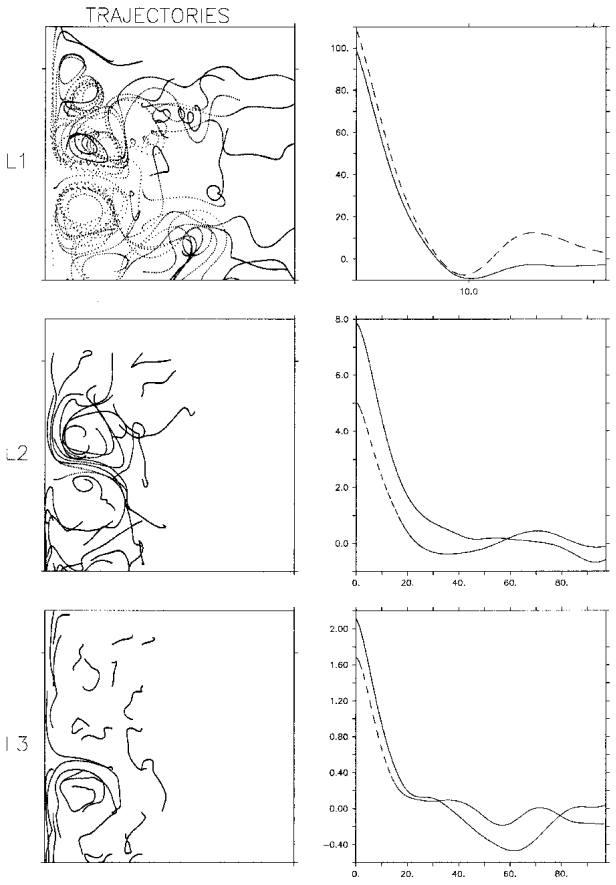

FIG. 3. (left column) Successive drifters positions (one point each half day) in each layer (L1, L2, L3). (right column) The corresponding Lagrangian autocovariance functions (in $cm^2\ s^{-2}$) vs time lag (in days). The solid (dashed) line shows the meridional (zonal) component.

The corresponding Lagrangian autocorrelation functions are plotted in the right-hand panels of Fig. 3. The Lagrangian time scale T_L, roughly estimated as the e-folding time scale of the autocorrelation, is about 5 days in L1 and about 15–20 days in L2 and L3. In comparison, ocean data show shorter values of T_L, especially in the upper ocean, where typical values are $T_L \approx 1$–3 days (e.g., Griffa 1996), while in the deep ocean $T_L \approx$ 7–15 days (e.g., Veneziani et al. 2004). Note that T_L can be considered as an indicator of the higher possible sampling frequency (or the minimum required sampling interval) for efficient assimilation. In Molcard et al. (2003), it is shown that there is an optimal range for the sampling period depending on the Lagrangian time scale, and that the assimilation is especially successful for $\Delta t < (T_L/2)$, while it becomes inefficient for $\Delta t > T_L$. This suggests that assimilation experiments (Table 2) with $\Delta t = 1200$ s and 3 days are likely to be successful for data taken in all the layers, while for $\Delta t = 6$ days the assimilation is expected to be inefficient for floats launched in the upper layer.

c. The analysis

The Assim and Noassim runs are initialized with the same initial condition. As mentioned in section 3d, the specific realizations of Assim and Noassim used here for visual comparison correspond to the 11Y initial condition (Table 2). Snapshots of layer thickness and horizontal velocity field at the initial and final times of the Noassim simulation are plotted in Fig. 4, while in Figs. 5–7 final results from three different Assim experiments are shown, corresponding to assimilation in three different layers (LaunchL1, LaunchL2, and LaunchL3) with $\Delta t = 3$ days (Table 2).

Results from the error metric (8) ϵ_{rel}, shown in Fig. 8, are used to quantitatively assess the assimilation performance, considering also the other Δt values. The metric is computed as an average over three different realizations with different initial conditions.

Let us start by discussing the results of LaunchL1. The results at the end of the assimilation (Figs. 5a–c) are to be compared with the true ocean state (Control) at the same time (Figs. 2d–f) and with the model without correction (Noassim) (Figs. 4d–f). The assimilation run resembles much more closely the Control than the Noassim, indicating that the assimilation has been successful and the correction of the velocity computed from the floats has been able to improve significantly the main patterns. The northwestern jet in L1 and L2 has been bended south and maintains a quasi-zonal direction as in the Control. The southern cyclonic gyre detached from the main jet present in the Noassim run in L1 and in L2 completely disappears in the corrected forecast. Finally, the swinging of the zonal jet in the Control is reproduced in all layers.

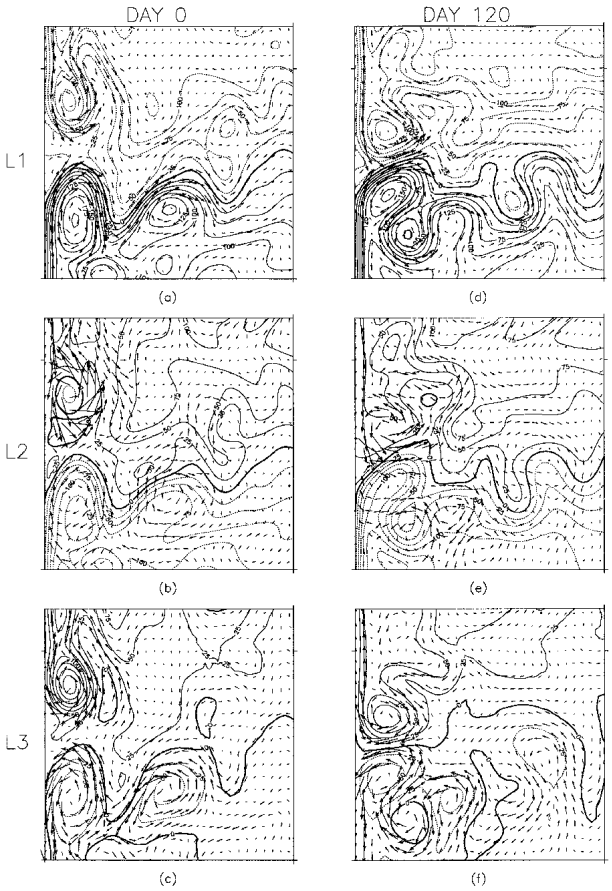

FIG. 4. Noassim run: layer thickness displacement ($h - h_{rest}$) superimposed on the velocity field in each layer (L1, L2, L3), at the initial time [DAY 0: (a)–(c)] and at the end [DAY 120: (d)–(f)] of the simulation. Contour intervals are 25 m, and the maximum velocity field is approximately 50 cm s^{-1} in L1, 10 cm s^{-1} in L2, and 5 cm s^{-1} in L3.

The results of LaunchL2, corresponding to assimilation of data in L2 (Fig. 6), are to be compared to Figs. 2 and 4. The improvement of the forecast appears weaker than that for LaunchL1, especially in L1, and it is more difficult to evaluate qualitatively. However, if we focus on the meandering zonal jet and the size of the main structures, the efficiency of the assimilation is apparent, especially in L2 and L3.

Finally, LaunchL3 leads to the results presented in Fig. 7. As expected, the best improvement is obtained in L3, where the data are directly measured and assimilated: the four-gyre structure clearly designed in the true ocean (Fig. 2f) has been completely reproduced. The high correlation between L1 and L3 guarantees good results also for L1, while for L2 the assimilation appears considerably less efficient.

It is interesting to note that the assimilation gives almost equally good results in the upper layer L1 when launching in L3 or in L1 (Fig. 5a and 7a, respectively). At closer inspection, however, even though the main patterns appear to be well reproduced in LaunchL3, the assimilation in LaunchL1 appears more efficient, especially in the eastern part of the region, as the floats are faster in L1, therefore covering the whole domain (Fig. 3).

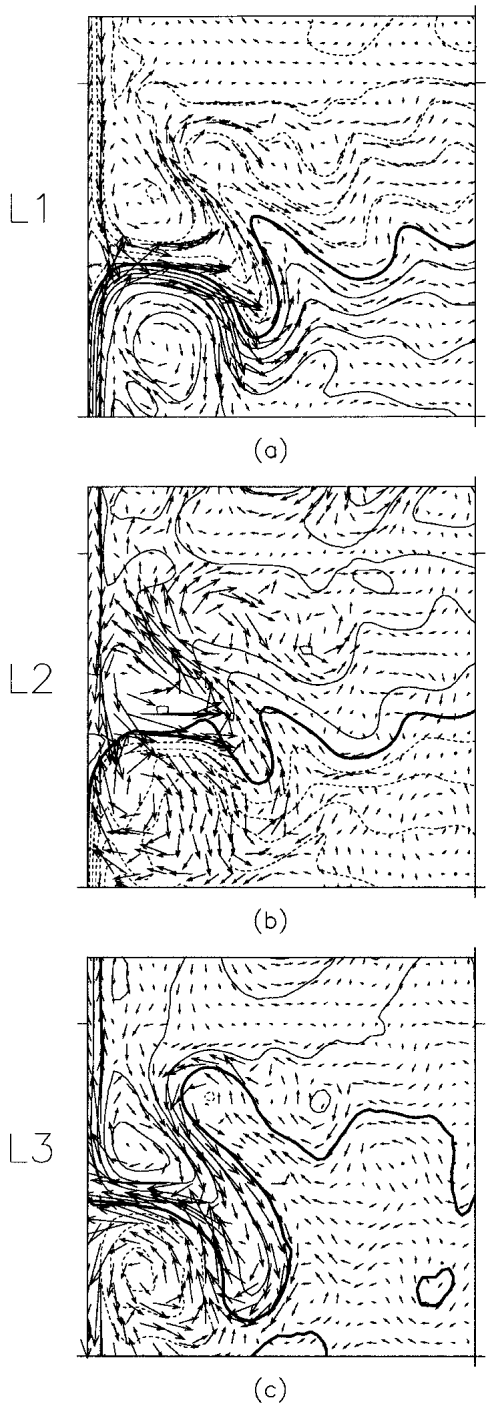

FIG. 5. Assim run expt LaunchL1, with assimilated data in L1: snapshots of layer thickness displacement and velocity field for each layer (L1, L2, L3) at the end of the simulation (DAY 120). Contour intervals are 25 m, and the maximum velocity field is approximately (a) 50 cm s^{-1} in L1, (b) 10 cm s^{-1} in L2, and (c) 5 cm s^{-1} in L3.

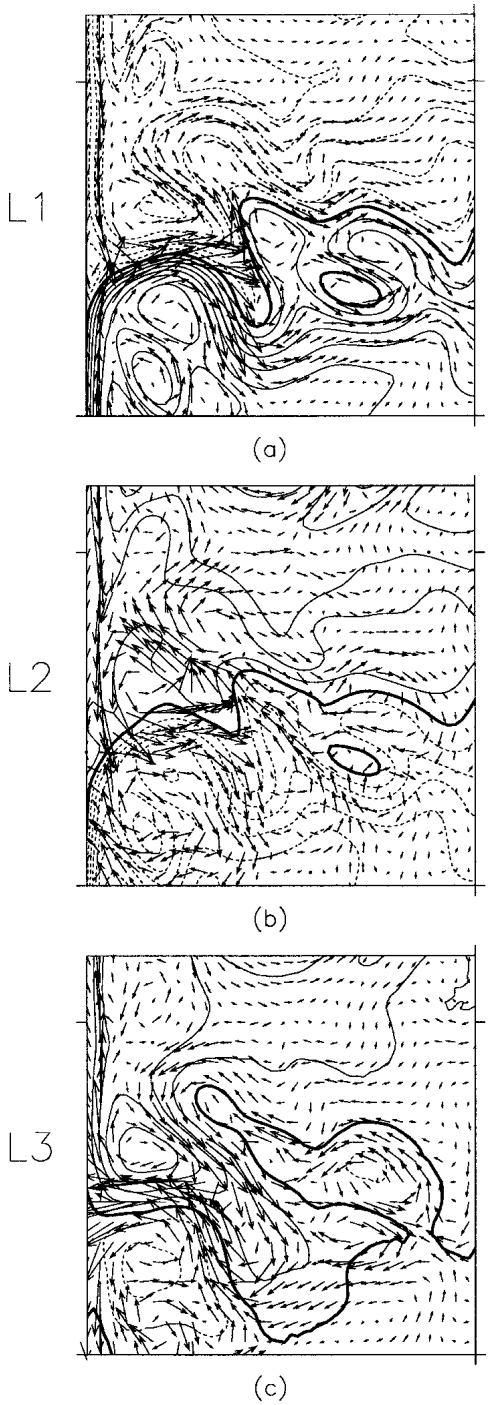

FIG. 6. Assim run expt LaunchL2, with assimilated data in L2: snapshots of layer thickness displacement and velocity field for each layer (L1, L2, L3) at the end of the simulation (DAY 120). Contour intervals are 25 m, and the maximum velocity field is approximately (a) 50 cm s^{-1} in L1, (b) 10 cm s^{-1} in L2, and (c) 5 cm s^{-1} in L3.

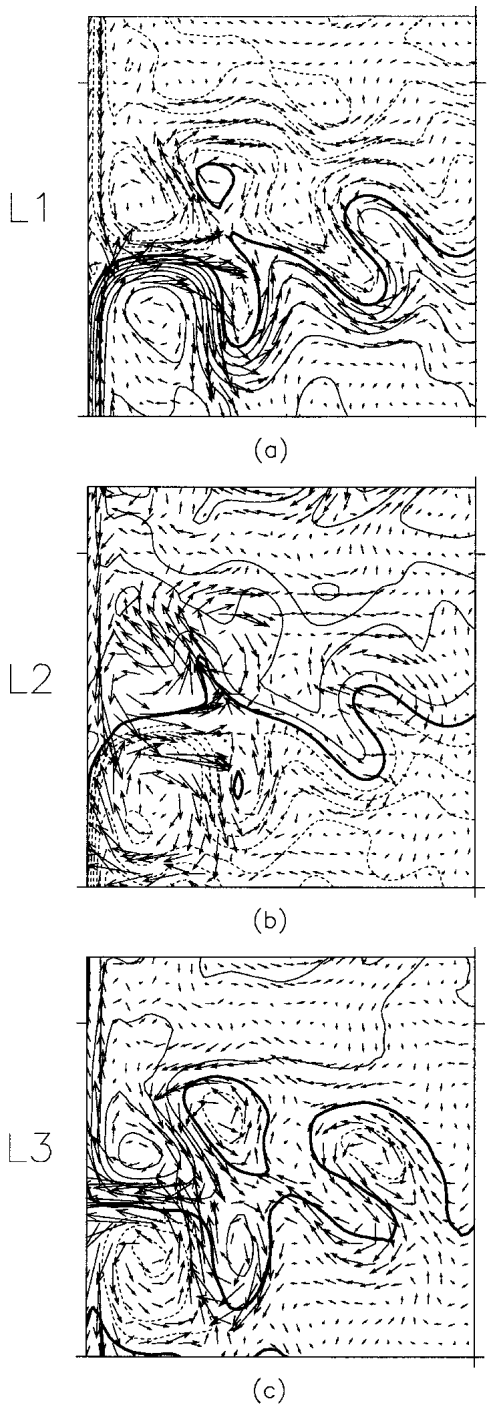

FIG. 7. Assim run expt LaunchL3, with assimilated data in L3: snapshots of layer thickness displacement and velocity field for each layer (L1, L2, L3) at the end of the simulation (DAY 120). Contour intervals are 25 m, and the maximum velocity field is approximately (a) 50 cm s^{-1} in L1, (b) 10 cm s^{-1} in L2, and (c) 5 cm s^{-1} in L3.

In summary, the qualitative comparison indicates that the assimilation method is effective and able to improve the forecast in all layers. This is particularly impressive considering that the method is at least partially based on the geostrophic assumption, and ageostrophic deviations are evident in L2 and L3.

In order to analyze more quantitatively the efficiency of the assimilation method, and to compare the whole

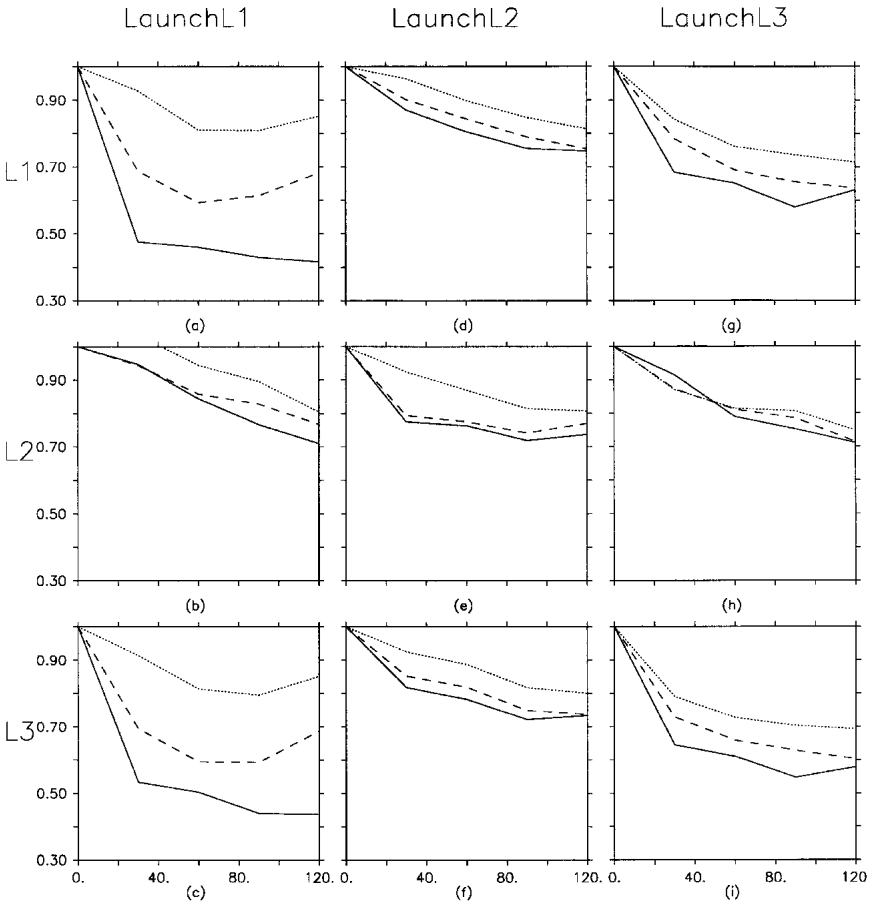

FIG. 8. Relative velocity error $\epsilon_{\text{rel}}(l, t)$ in each layer (L1, L2, L3) for the three launchings. [LaunchL1 (a)–(c), LaunchL2 (d)–(f), and LaunchL3 (g)–(i)]. The three lines in each figure show results from different sampling periods Δt: 1200 s (solid), 3 days (dashed), and 6 days (dotted).

set of experiments in terms of launching layer and sampling period Δt, we consider the time evolution of the relative errors $\epsilon_{rel}(l, t)$ computed from (8). The behavior of $\epsilon_{rel}(l, t)$ for the various experiments is shown in Fig. 8. Each column represents a specific experiment (LaunchL1, LaunchL2, or LaunchL3), while each row refers to the layer where the metric is computed. In each panel, the three lines represent results for a different sampling period Δt (the dashed line corresponds to $\Delta t = 3$ days, as in Figs. 5–7).

The first evidence from this figure is that in all cases the assimilation improves the forecast as the relative error reduces consistently in all experiments until $t \approx 90$ days, after which the assimilation performance may level off or reduce in some cases due to decreasing space sampling density when drifters start leaving the target region. The dependence on the sampling period is especially strong for the experiment LaunchL1. This is in agreement with the results from Molcard et al. (2003), who have shown that the assimilation is especially efficient for $\Delta t < (T_L/2)$ and deteriorates for $\Delta t > T_L$. Since $T_L \approx 5$ days in L1, it is not surprising that the error increases from $\Delta t = 1200$ s to $\Delta t = 3$ days, and it reaches values of ≈80%–90% for $\Delta t = 6$ days. In the deeper layers L2 and L3, instead, the time scale $T_L \approx$ 15–20 days; that is, it is significantly longer than all the considered Δt. As a consequence the degradation of the assimilation efficiency with increasing sampling period is very slow.

The best results in terms of minimizing ϵ_{rel} are achieved when launching in L1 and when the assimilation procedure is applied at each time step with a final error in L1 and L3 around 40%. This is probably due to the fact that the surface flow is the most energetic, so that is able to significantly correct the velocity field, and it is strongly correlated with the third-layer velocity, allowing for a significant correction also in L3.

The error in L2 is almost independent of the launching, and it remains around 70% for all the experiments. This is due to the reduced correlation between L2 and the other layers (Table 3), which affects the assimilation efficiency, in agreement with previous results (Chin et al. 2002).

All together, the launching in L3 gives the best av-

eraged result, as the improvement of the forecast is consistent in all layers, even at high sampling period, and the difference between the crude forecast and the true ocean has been reduced by almost a factor of 2, at least in the third layer.

Notice the rapid convergence in the first month, which is present in all the experiments, although to different degrees. This indicates that the assimilation is highly effective in the initial phase, when differences between the crude forecast and the real ocean are important.

As an important final remark, we notice that in order to interpret the results on the Δt dependence for real ocean applications, we should renormalize the results in terms of ocean values for T_L. For ocean surface, with $T_L \approx$ 1–3 days, the assimilation is expected to be especially efficient for $\Delta t <$ 0.5–1.5 days, while for deep ocean, with $T_L \approx$ 7–15 days, $\Delta t <$ 3.5–7 days. Assimilation with $\Delta t >$ 10 days is likely to be inefficient.

5. Summary and concluding remarks

In this study, a method to assimilate Lagrangian position data in multilayer OGCMs is presented. The method directly builds on the results of Molcard et al. (2003) for the correction of the Eulerian velocity in the same layer where the Lagrangian data are measured. Regarding the projection to other layers and other variables, an approach similar to those of Oschlies and Willebrand (1996) and to Özgökmen et al. (2003) is used, based on statistical regression for the velocity correction, and on geostrophy and mass balance for the layer thickness.

The method can be summarized in terms of the following successive steps.

1) The Eulerian velocity is corrected in the same layer where Lagrangian data are measured, minimizing the difference between observed and simulated Lagrangian velocity during the sampling period Δt. The simulated Lagrangian velocity is computed by advecting synthetic floats in the model velocity field.
2) The velocity correction in the other layers is computed using statistical regression coefficients between layers. These coefficients are computed from model outputs as time and spatial averages.
3) The layer thickness is corrected in each layer using a dynamical balancing technique based on geostrophy and mass conservation.

This general approach has been applied and tested using a three-layer MICOM primitive equation model in a double-gyre configuration and a set of twin experiments. In all cases, the floats have been released in the most energetic western region. The assimilation efficiency is first tested qualitatively by comparing snapshots of the Control and Assim runs, while a more quantitative assessment is done using a relative error metric. In particular, the efficiency of the assimilation has been tested for launches in the various layers and for different values of Δt. Three values of Δt have been considered: Δt = 1200 s, 3 days, and 6 days.

The first layer is the most energetic and is characterized by the fastest time scale (T_L = 5 days). When the assimilated data are taken in the first layer and Δt is small (Δt =1200 s), the assimilation is very efficient and gives errors as low as of ≈40% in the first and third layers after 120 days of assimilation. At increasing Δt, the assimilation efficiency decreases, reaching errors of ≈80% for Δt = 6 days.

When data collected in the third layer are assimilated, the results are still satisfactory, with errors < 60% and a good visual agreement between snapshots of Control and Assim. The dependence of the results on Δt is distinctively less marked than for the case with first-layer assimilation. This is due to the fact that the time scales of the deeper layers are longer ($T_L \approx$ 15–20 days), so that Δt is always smaller than the Lagrangian time scale T_L.

Results for assimilation of data taken in the second layer show a similar insensitivity to Δt (since the T_L values are similar), but the errors are higher, exceeding 70%. Also, the visual comparison is less satisfactory. This is due to the fact that the second layer is less correlated than the other two, in agreement with what was also found by Chin et al. (2002).

All together, the results are encouraging and suggest that Lagrangian data assimilation might be effective in stratified OGCMs. Of course, the assimilation efficiency appears to be strongly tied to the degree of vertical correlation, so that the results can be expected to vary significantly, depending on the characteristics of the current system sampled by the floats. On the other hand, the experiments show that, if the correlation is high, even the assimilation of deep layers with low energetics can be very effective. Also, even though the method is partially based on geostrophy, it appears robust to significant ageostrophic deviations, which are present in the deeper layers of the simulated flow.

The present results cannot be used directly to provide indications for oceanic applications, since the model is very simple and only partially realistic. Time scales appear longer than in the real ocean, and the eddy field is smoother and characterized by an unrealistically baroclinic vertical structure with respect to real eddies in extension jets. On the other hand, the results indicate the feasibility of the assimilation and encourage exploration of more complex models and applications, while providing some general suggestions on parameter ranges for applications. Regarding the dependency on the sampling period Δt, the results confirm the conclusions presented in Molcard et al. (2003). The assimilation appears especially effective for $\Delta t < T_L/2$, while it deteriorates for $\Delta t > T_L$. Based on these results, some general recommendations can be made for sampling periods in oceanic flows: optimal Δt should be

of the order of 0.5–1.5 days at the ocean surface ($T_L \approx$ 1–3 days), and of the order of 3.5–7 days in the ocean interior ($T_L \approx$ 7–15 days). Sampling periods Δt greater than 10 days are likely to be very ineffective for practical applications.

As a final remark, we notice that the present work points out a number of interesting issues that merit further investigation. For practical applications involving profiling float assimilation, for instance, further studies on the impact of data errors are necessary. In this paper, the data error is assumed constant and due to position recording uncertainty. For profiling floats, on the other hand, the error depends on vertical shear and surface drift and therefore is likely to be spatially varying and dependent on the specific current system. Also, specific methods to correct and reduce this error can be developed. Surface drift, for instance, can be corrected extrapolating from multiple position measurements, as shown by Davis et al. (1992) and Schmid et al. (2001), while vertical shear effects might be partially corrected using model or data results. At a more general level, future studies will have to address the question of how to partition information into temperature and salinity corrections (Oschlies and Willebrand 1996; Cooper and Haines 1996), and how to assimilate simultaneous data information, such as *T*/*S* profiles or satellite data, involving multivariate techniques.

Acknowledgments. The authors greatly appreciate the support of the Office of Naval Research under Grant N00014-03-1-0285 (A. Molcard, A. Griffa, and T. M. Özgökmen) and of the EU project MFSTEP (A. Molcard and A. Griffa).

REFERENCES

Bauer, S., M. S. Swenson, and A. Griffa, 2002: Eddy mean flow decomposition and eddy diffusivity estimates in the tropical Pacific Ocean: 2. Results. *J. Geophys. Res.,* **107,** 3154, doi:10.1029/2000JC000613.

Bleck, R., and D. B. Boudra, 1986: Wind-driven spin-up eddy-resolving ocean models formulated in isopycnic and isobaric coordinates. *J. Geophys. Res.,* **91C,** 7611–7621.

——, H. P. Hanson, D. Hu, and E. B. Kraus, 1989: Mixed layer–thermocline interaction in a three-dimensional isopycnic coordinate model. *J. Phys. Oceanogr.,* **19,** 1417–1439.

Carter, E. F., 1989: Assimilation of Lagrangian data into a numerical model. *Dyn. Atmos. Oceans,* **13,** 335–348.

Chin, T. M., A. C. Haza, and A. J. Mariano, 2002: A reduced-order information filter for multi-layer shallow water models: Profiling and assimilation of sea surface height. *J. Atmos. Oceanic Technol.,* **19,** 517–533.

Cooper, M., and K. Haines, 1996: Altimetric assimilation with water property conservation. *J. Geophys. Res.,* **101,** 1059–1077.

Davis, R. E., 1991: Observing the general circulation with floats. *Deep-Sea Res.,* **38,** 5531–5571.

——, D. C. Webb, L. A. Regier, and J. Dufour, 1992: The autonomous Lagrangian current explorer. *J. Atmos. Oceanic Technol.,* **9,** 264–285.

——, J. T. Sherman, and J. Dufour, 2001: Profiling Alace and other advances in autonomous subsurface floats. *J. Atmos. Oceanic Technol.,* **18,** 982–993.

Demirov, E., N. Pinardi, P. De Mey, M. Tonani, and C. Fratianni, 2003: Assimilation scheme of Mediterranean forecasting system: Conceptual basis and applications. *Ann. Geophys.,* in press.

Fratantoni, D. M., 2001: North Atlantic surface circulation during the 1990's observed with satellite-tracked drifters. *J. Geophys. Res.,* **106,** 22 067–22 093.

Ghil, M., and P. Malanotte-Rizzoli, 1991: Data assimilation in meteorology and oceanography. *Advances in Geophysics,* Vol. 33, Academic Press, 141–266.

Greiner, E., and S. Arnault, 2000: Comparing the results of a 4-D variational assimilation of satellite and in-situ data with WOCE CITHER hydrographic measurements in the tropical Atlantic. *Progress in Oceanography,* Vol. 47, Pergamon, 1–68.

Griffa, A., 1996: Applications of stochastic particle models to oceanographic problems. *Stochastic Modeling in Physical Oceanography,* R. Adler, P. Muller, and B. Rozovskii, Eds., Birkhauser, 113–128.

Hernandez, F., P. Y. Le Traon, and N. H. Barth, 1995: Optimizing a drifter cast strategy with a genetic algorithm. *J. Atmos. Oceanic Technol.,* **12,** 330–345.

Ide, K., L. Kuznetsov, and C. K. R. T. Jones, 2002: Lagrangian data assimilation for point vortex systems. *J. Turbulence,* **3,** 053, doi:10.1088/1468-5248/3/1/053.

Ishikawa, Y. I., T. Awaji, and K. Akimoto, 1996: Successive correction of the mean sea surface height by the simultaneous assimilation of drifting buoy and altimetric data. *J. Phys. Oceanogr.,* **26,** 2381–2397.

Kamachi, M., and J. J. O'Brien, 1995: Continuous assimilation of drifting buoy trajectory into an equatorial Pacific Ocean model. *J. Mar. Syst.,* **6,** 159–178.

Killworth, P. D., C. Dieterich, C. Le Provost, A. Oschlies, and J. Willebrand, 2001: Assimilation of altimetric data and mean sea surface height into an eddy-permitting model of the North Atlantic. *Progress in Oceanography,* Vol. 48, Pergamon, 313–335.

Kuznetsov, L., K. Ide, and C. K. R. T. Jones, 2003: A method for assimilation of Lagrangian data. *Mon. Wea. Rev.,* **131,** 2247–2260.

Lavender, K. L., R. E. Davis, and W. B. Owens, 2000: Mid-depth recirculation observed in the Labrador and Irminger Ses by direct velocity measurements. *Nature,* **407,** 66–69.

——, ——, and ——, 2002: Observations of open ocean deep convection in the Labrador Sea from subsurface floats. *J. Phys. Oceanogr.,* **32,** 511–526.

Li, J. G., P. D. Killworth, and D. A. Smeed, 2003: Response of an eddy-permitting ocean model to the assimilation of sparse in situ data. *J. Geophys. Res.,* **108,** 3111, doi:10.1029/2001JC001033.

Mariano, A. J., A. Griffa, T. M. Özgökmen, and E. Zambianchi, 2002: Lagrangian analysis and predictability of coastal and ocean dynamics 2000. *J. Atmos. Oceanic Technol.,* **19,** 1114–1125.

Masina, S., N. Pinardi, and A. Navarra, 2001: A global ocean temperature and altimeter data assimilation for studies of climate variability. *Climate Dyn.,* **17,** 687–700.

Miyakoda, K., J. Smagorinski, R. F. Strickler, and G. D. Hembree, 1969: Experimental extended predictions with a nine-level hemispheric model. *Mon. Wea. Rev.,* **97,** 1–76.

Molcard, A., L. I. Piterbarg, A. Griffa, T. M. Özgökmen, and A. J. Mariano, 2003: Assimilation of drifter positions for the reconstruction of the Eulerian circulation field. *J. Geophys. Res.,* **108,** 3056, doi:10.1029/2001JC001240.

Oschlies, A., and J. Willebrand, 1996: Assimilation of Geosat altimeter data into an eddy-resolving primitive equation model of the North Atlantic Ocean. *J. Geophys. Res.,* **101** (C6), 14 175–14 190.

Owens, W. B., 1991: A statistical description of the mean circulation and eddy variability in the northwestern Atlantic using SOFAR floats. *Progress in Oceanography,* Vol. 28, Pergamon, 257–303.

Özgökmen, T. M., A. Molcard, T. M. Chin, L. I. Piterbarg, and A. Griffa, 2003: Assimilation of drifter positions in primitive equation models of midlatitude ocean circulation. *J. Geophys. Res.,* **108,** 3238, doi:10.1029/2002JC001719.

Poje, A. C., M. Toner, A. D. Kirwan Jr., and C. K. R. T. Jones, 2002: Drifter launch strategies based on Lagrangian templates. *J. Phys. Oceanogr.,* **32,** 1855–1869.

Raicich, F., and A. Rampazzo, 2003: Observing system simulation experiment for the assessment of temperature sampling strategies in the Mediterranean Sea. *Ann. Geophys.,* **21,** 151–165.

Reverdin, G., P. P. Niiler, and H. Valdimasson, 2003: North Atlantic Ocean surface currents. *J. Geophys. Res.,* **108,** 3002, doi:10.1029/2001JC001020.

Richardson, P. L., 2001: Drifters and floats. *Encyclopedia of Ocean Sciences,* Vol. 2, Academic Press Ltd., 767–774.

Robinson, A. R., and P. F. J. Lermusiaux, 2001: Data assimilation in models. *Encyclopedia of Ocean Sciences,* Academic Press Ltd., 623–634.

Schmid, C., B. Molinari, and S. Garzoli, 2001: New observations of the intermediate depth circulation in the tropical Atlantic. *J. Mar. Res.,* **59,** 281–312.

Thacker, W. C., and O. E. Esenkov, 2002: Assimilating XBT data into HYCOM. *J. Atmos. Oceanic Technol.,* **19,** 709–724.

Toner, M., A. D. Kirwan, L. H. Kantha, and J. K. Choi, 2001a: Can general circulation models be assessed and their output enhanced with drifter data? *J. Geophys. Res.,* **106,** 19 563–19 579.

——, A. C. Poje, A. D. Kirwan, C. K. R. T. Jones, B. L. Lipphardt, and C. E. Grosch, 2001b: Reconstructing basin-scale Eulerian velocity fields from simulated drifter data. *J. Phys. Oceanogr.,* **31,** 1361–1376.

Veneziani, M., A. Griffa, A. M. Reynolds, and A. J. Mariano, 2004: Oceanic turbulence and stochastic models from subsurface Lagrangian data for the Northwest Atlantic Ocean. *J. Phys. Oceanogr.,* **34,** 1884–1906.

Zhang, H. M., M. D. Prater, and T. Rossby, 2001: Isopycnal Lagrangian statistics from the North Atlantic Current RAFOS float observations. *J. Geophys. Res.,* **106,** 13 817–13 836.

Zhou, M., P. P. Niiler, and J. H. Hu, 2002: Surface currents in the Bransfield and Gerlache Straits, Atlantica. *Deep-Sea Res.,* **49,** 267–280.